Acoustic phonon Raman scattering induced by a built-in electric field

G. Rozas,[1] M. F. Pascual Winter,[1,2] A. Fainstein,[1,*] B. Jusserand,[2] P. O. Vaccaro,[3,†] and S. Saravanan[3]
[1]*Centro Atómico Bariloche & Instituto Balseiro, CNEA, R8402AGP S. C. de Bariloche, Río Negro, Argentina*
[2]*Institut des Nanosciences de Paris, UMR CNRS 7588, Université Pierre et Marie Curie, Campus Boucicaut, 140 Rue de Lourmel, 75015 Paris, France*
[3]*ATR Wave Engineering Laboratories, 2-2-2 Hikaridai, Keihanna Science City, Kyoto 619-0288, Japan*
(Received 6 September 2007; revised manuscript received 19 December 2007; published 9 April 2008)

We report acoustic phonon resonant Raman scattering experiments in strained piezoelectric [311] $Ga_{0.85}In_{0.15}As/AlAs$ superlattices with permanent built-in piezoelectric fields. The acoustic phonon spectra develop upon resonant excitation around the "forbidden" $hh_2 \rightarrow e_1$ interband transition into a broad intense structure, which is peaked at the first folded phonons. Standard narrow acoustic phonon doublets are recovered when the power of the resonant laser excitation is increased. Such change in the resonant Raman spectra with increasing power is accompanied by a strong shift and bleaching of a photoluminescence emission related to the $hh_2 \rightarrow e_1$ transition. None of these observations are present in [001] $Ga_{0.85}In_{0.15}As/AlAs$ superlattices that lack the built-in fields because of symmetry. We interpret these results as originated in a Raman process resonant with an intermediate transition that becomes allowed due to the built-in fields. We address the possible mechanisms by which the acoustic phonons strongly modulate the dielectric function in these piezoelectric nanostrutures, including an electron-acoustic-phonon interaction involving the phonon modulation of the built-in fields. This mechanism, which is shown to be proportional to the magnitude of the built-in fields, is quenched when the latter are screened by photoexcited carriers.

DOI: 10.1103/PhysRevB.77.165314 PACS number(s): 78.30.Fs, 63.20.D−, 78.66.Fd, 42.60.Da

"Nanophononics," which is the domain of acoustic phonons of gigahertz-terahertz frequencies and nanometer wavelengths, is relevant for the manipulation of sound and heat at the nanoscale. Through the electron-phonon interaction, such phonon engineering has implications on the control of charge and light at high frequencies and with reduced dimensions. Important progress has lately emerged in the development of nanowave phononic devices including, e.g., mirrors, cavities, and monochromatic sources.[1–5] The deformation potential interaction that couples acoustic phonons and electrons is, however, relatively weak. This fact introduces an intrinsic limitation for the development of multifunctional acoustic devices designed to act on electronic or optical properties.

One alternative to overcome this limitation involves the piezoelectric coupling in noncentrosymmetric materials. It turns out, however, that the electron-acoustic phonon coupling through the piezoelectric interaction in III-V semiconductors is also relatively weak, which leads to minor changes in the electron and phonon lifetimes, sound velocities, and Raman cross sections. It has been recently pointed out that a different situation may arise when built-in *permanent* piezoelectric fields are present.[6–10] Interestingly, a huge acoustic phonon coherent generation efficiency has been reported in GaInN/GaN piezoelectric superlattices (SLs), which is more than 2 orders of magnitude larger than that observed in standard GaAs/AlAs structures.[6,7] The proposed mechanism involves the screening of the piezoelectric built-in field by photoexcited carriers, which triggers an instantaneous coherent displacement with wave vector determined by the SL period.[8] These results suggest that the modulation of the built-in fields by the acoustic phonon strain should open an additional channel of electron-acoustic-phonon coupling that could, in principle, be tailored and dynamically controlled.[10] In this paper, we report the first observation of electric-field induced Raman scattering by acoustic phonons in strained [311] $Ga_{0.85}In_{0.15}As/AlAs$ superlattices with permanent built-in piezoelectric fields. We demonstrate that the Raman process is strongly resonant with a *forbidden* interband transition involving the second confined heavy-hole (hh_2) and the first confined electron (e_1) levels. Most interestingly, a quenching of this resonance is observed with increasing laser power, which demonstrates that the Raman process can be tuned by screening the built-in piezoelectric fields with photoexcited carriers. Possible mechanisms by which the acoustic phonons can strongly modulate the dielectric function in the presence of built-in fields (thus leading to the Raman scattered light) are addressed.

Polar III-V semiconductors, which are noncentrosymmetric materials and thus intrinsically piezoelectric, may display permanent built-in electric fields along the growth direction when grown in multilayers that are strained by lattice mismatch. Structures grown along [001] do not possess permanent piezoelectric fields because of symmetry, while very large fields (up to $\approx 10^5$ V/cm) are present for almost any other growth direction.[11] To investigate the role of these permanent piezoelectric fields on the Raman scattering by acoustic vibrations, we have performed a comparative study of $Ga_{0.85}In_{0.15}As/AlAs$ SLs grown both along [001] and [311]. The thickness of the 24 $Ga_{0.85}In_{0.15}As/AlAs$ layers, which are designed to have the first zone-center acoustic phonon minigap at ~ 18 cm^{-1}, were 21 Å/78 Å(23 Å/84 Å) for the [001]([311]) SL. A 1 μm $Ga_{0.44}Al_{0.56}As$ alloy sacrificial layer was grown between the SLs and the GaAs substrate to eventually allow the chemical etching of the substrate. The excellent quality of the structures was evidenced by the observation of up to seven (five) doublets in the acoustic folded phonon Raman spectra.[10] High resolution x-ray diffraction displays several SL satellites and indicates that the layers are pseudomorphic with the

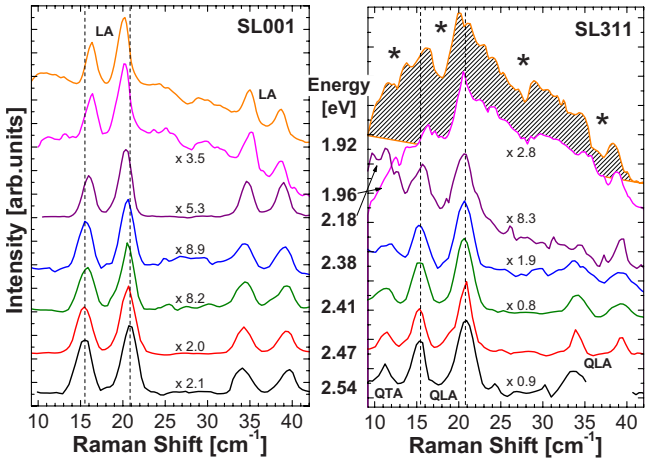

FIG. 1. (Color online) Acoustic phonon Raman spectra taken at 80 K for various laser lines of an Ar-Kr ion laser. Left: [001] SL. Right: [311] SL. The shaded region in the top spectrum of the right panel highlights the broad intense background that appears for the [311] sample at 1.96 and 1.92 eV.

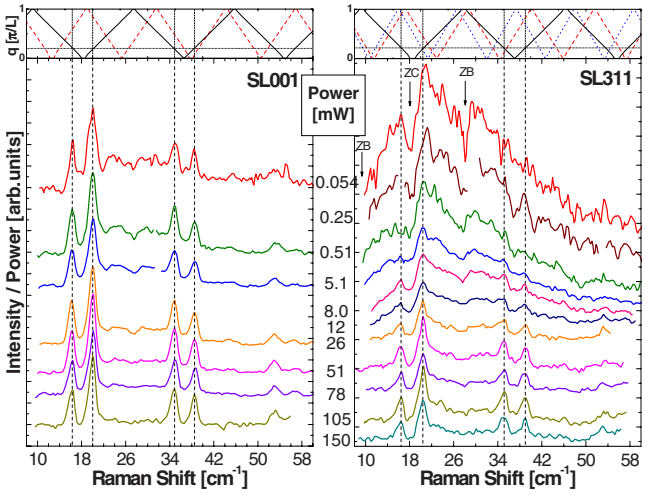

FIG. 2. (Color online) Folded acoustic phonon spectra taken with 1.92 eV resonant excitation with powers ranging from ~50 μW to ~150 mW. The spectra in the figure have been normalized to the incident power and an exponential tail has been subtracted. Left panel: [001] SL. Right panel: [311] SL. The top panels present the acoustic phonon dispersion calculated by using a continuum Rytov model for the LA (solid), TA (dashed), and QTA (dotted) phonons. ZC and ZB label the features related to zone-center and zone edge gaps, respectively.

substrate and ~2% thinner than the nominal values (in agreement with the Raman data). Strain relaxation, if any, should be below 0.5% (one dislocation every 3 μm). It thus follows that the AlAs layers are only weakly strained (≈0.05%), while $Ga_{0.85}In_{0.15}As$ is under a large (≈1%) compressive in-plane strain. We have estimated the polarization charges and built-in electric fields following Ref. 11. By assuming a complete absence of dislocations and boundary conditions appropriate for a quasi-infinite SL (the electric potential averages to zero in every $Ga_{0.85}In_{0.15}As/AlAs$ bilayer), the built-in electric fields can be estimated to be $F \approx 0.5 \times 10^5$ V/cm in the $Ga_{0.85}In_{0.15}As$ layers.[11]

Figure 1 displays acoustic phonon Raman spectra, which are taken at 80 K for various lines of an Ar-Kr ion laser, with parallel incident and scattered polarizations. In all cases, the laser power was 5 mW, which is focused on a ~30 μm spot. The collected spectra were dispersed by using a Jobin-Yvon T64000 spectrometer and detected with a liquid-N_2-cooled charge coupled device. For [001] oriented structures, there are two degenerate transverse acoustic (TA) and one longitudinal acoustic (LA) branches. For [311] grown structures, three nondegenerate branches exist, where one is purely transverse (TA), another is quasitransverse (QTA), and the third is quasilongitudinal (QLA). As illustrated in Fig. 1, for all laser energies in the [001] structure but only at high energies for the [311] oriented sample, narrow folded acoustic phonon peaks are clearly observed. In agreement with the Raman selection rules, only LA modes are observed along [001], while both QLA and QTA modes appear for polarized backscattering along [311].[10,12] The spectra qualitatively change for the [311] oriented structure when the laser energy is decreased. Already for 2.18 eV, a laserlike tail develops, which turns into a broad intense background at 1.96 and 1.92 eV (see the shaded spectrum highlighted in Fig. 1). Concomitant with the appearance of this background, the folded acoustic peaks shift, broaden, and wash out, and new peak and diplike features develop (these are marked with asterisks in Fig. 1).

The results displayed in Fig. 1 suggest that a resonant contribution to the Raman cross section is active for the [311] sample but absent for the [001] orientation. This resonant process displays a strikingly unusual power dependence, as shown for 1.92 eV resonant excitation in Fig. 2 for powers ranging from ~50 μW to ~150 mW. The spectra in the figure have been normalized to the incident power. An exponential tail, which is produced by the resonance with the fundamental (lower energy) transition and evident in the top spectra of Fig. 1, has been subtracted from every spectra on both samples. For the SL grown along [001] (left panel), the normalized Raman spectra are essentially independent of laser power, as expected. In contrast, the [311] structure (right panel) presents spectra that vary from the typical narrow doublets at high powers (bottom) to a large broad background at low powers (top). Similar to the spectra in Fig. 1, with decreasing power besides the appearance of the intense broad background, the doublets broaden and shift, and additional peaks and dips can be clearly observed (indicated with arrows in the figure). We also present at the top of Fig. 2 the acoustic phonon dispersion calculated by using a continuum Rytov model,[13] with the material parameters from Ref. 12. It can be deduced from this figure that the large observed background corresponds to acoustic phonons coming from the whole Brillouin zone, while the additional peaks and dips can be identified with regions of higher and lower density of states, respectively, in the phonon dispersion (center and edge of the Brillouin zone).[14]

The observation of acoustic phonons from the whole Brillouin zone, including dips and peaks associated with the peculiarities of the phonon dispersion, was quite thoroughly discussed by Ruf *et al.*[15] Their studies clearly established that wave vector nonconservation related to disorder and a

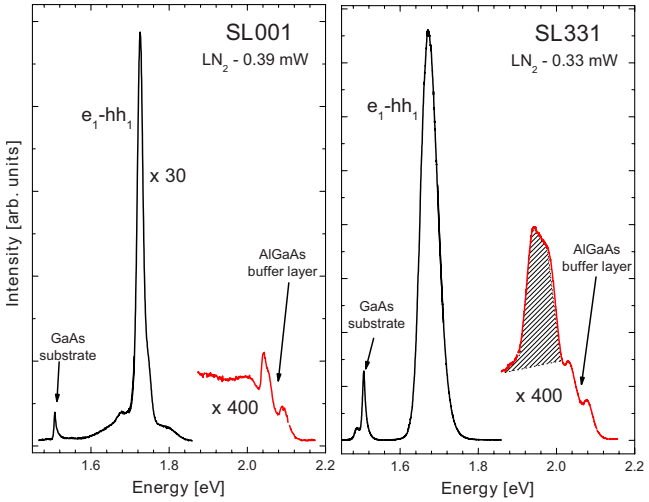

FIG. 3. (Color online) Photoluminescence measurements obtained for the [001] and [311] superlattices at 80 K and with 488 nm excitation.

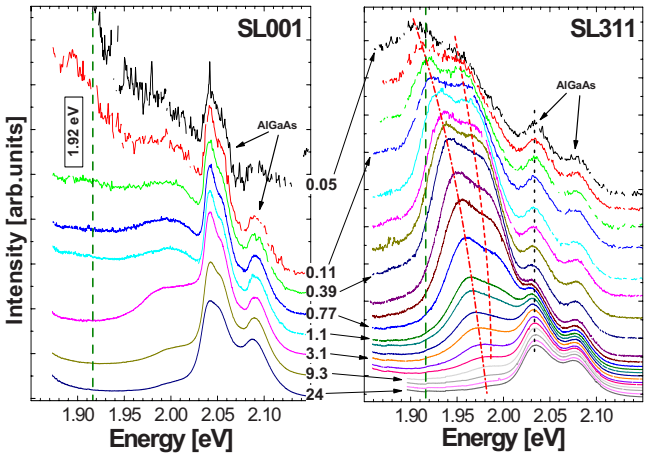

FIG. 4. (Color online) Photoluminescece measurements in the spectral region close to the energy of the $hh_2 \rightarrow e_1$ transition performed both in the [001] and [311] SLs at 80 K and for different excitation powers ranging from ≈ 50 μW (top) to ≈ 24 mW (bottom). The numbers indicate the incident power in mW. All curves have been normalized to display the same intensity of the peaks at ≈ 2.05, which originated in the $Ga_{0.44}Al_{0.56}As$ sacrificial alloy layer. The vertical line at 1.92 eV in the left panel indicates the laser energy used for the resonant spectra displayed in Fig. 2. The lines in the right panel are guides to the eyes.

strong Raman resonance are at the origin of such kind of features. Briefly stated, when the laser energy is away from resonance, the collection of quantum wells (QWs) contributing to the Raman polarization are basically equivalent and, consequently, their periodicity leads to a defined wave vector in the scattered light. Under these circumstances, narrow doublets are observed. On the other hand, when the laser is within or close to an inhomogeneously broadened distribution of QW states, each of the states differently contribute to the scattered light, those closer to the laser being more intense because of resonance. The interference of the scattered light thus loses coherence, the spectra reflect features belonging to scattering by individual QWs, and, for this reason, the wave vector is not conserved. The peculiarity of the results presented here is that such Raman resonance involving acoustic phonons is observed in a "forbidden" transition due to the presence of built-in electric fields, a resonance that can be tuned, and fully bleached, by increasing the laser power.

The presence of large permanent strain-induced fields modifies the potential landscape sensed by carriers, which changes in a fundamental way the optical properties of these structures. To begin with, the electric fields shift the confined energy levels through the quantum confined Stark effect.[16,17] In addition, optical transitions that are otherwise forbidden by symmetry become allowed. In the absence of electric field, the envelope functions of the confined states are either even or odd. Consequently, optical transitions are only allowed between electron and hole levels of the same parity. The electric field removes the reflection symmetry and, consequently, also the parity selection rule. Figure 3 presents photoluminescence measurements obtained for the two studied samples at 80 K. A detail of these photoluminescence measurements which correspond to the spectral region where the strong resonant behavior is observed in Figs. 1 and 2 is presented in Fig. 4. The latter are shown for different powers of the 488 nm excitation laser (2.54 eV). The peaks observed in these spectral region are more than 2 orders of magnitude weaker than the fundamental first heavy-hole to first electron ($hh_1 \rightarrow e_1$) transition (observed at $\sim 1.7-1.72$ eV for the [001] SL in Fig. 3). For the [001] sample (left panel in Fig. 4), the spectra are basically independent of laser power, and are mainly characterized by the doublet localized at ≈ 2.05 and ≈ 2.09 eV which is due to indirect $\Gamma - X$ transitions in the $Ga_{0.44}Al_{0.56}As$ sacrificial alloy layer. All curves in Fig. 4 have been normalized to display the same intensity of the peak at ≈ 2.05.

The same kind of power-independent structure is also observed for the [311] structure (right panel of Fig. 4). In addition, at low excitations, the spectra display a relatively intense double peak (at ~ 1.9 and ~ 1.95 eV) that is not present in the [001] sample. With increasing power, this structure strongly blueshifts (~ 60 meV), reduces its splitting, and decreases its relative intensity until it is almost unobservable for incident power ≥ 15 mW. According to a standard calculation of electronic states with an effective mass envelope function model,[17] this feature can be related to the second heavy-hole to first confined electron ($hh_2 \rightarrow e_1$) transition (calculated to appear at ≈ 1.99 eV). As a reference, we note that the fundamental gap is predicted to fall at ≈ 1.74 eV (not including any excitonic correlation). In the [001] SL, this transition (either direct or to neighbor wells) is forbidden by symmetry. For the [311] structure, on the other hand, the built-in fields lead to finite transition probabilities. With increasing laser power, photoexcited carriers screen the built-in fields, thus recovering the parity conservation selection rules that characterizes the [001] sample. We have calculated the density of free electrons required to fully screen the built-in fields to be $\approx 4 \times 10^{17}$ cm^{-3}. Following Ref. 18, we have estimated that these densities are reached in our samples with an incident power of a few milliwatts, which is in very good agreement with the power dependence of the Raman and photoluminescence spectra

displayed in Figs. 2 and 4, respectively. The observed power dependent shift of ≈ 60 meV, on the other hand, is too large to be solely accounted for by the quantum confined Stark effect in our relatively narrow 21 Å GaAs QWs. A field-dependent coupling to the X states in the AlAs barrier, which fall approximately at the same energy, could be contributing to this large effect. In any case, it is apparent that the resonance with this strongly field-dependent transition leads to the notable Raman behavior displayed in Figs. 1 and 2. The mechanisms by which this phenomenon occurs will be discussed next.

The Raman efficiency for scattering by acoustic phonons is given by[17]

$$I(\omega) \propto \left| \int dz E_L E_S^* \frac{\partial \chi}{\partial \varepsilon} \Delta\epsilon \right|^2, \tag{1}$$

where $E_L(E_S)$ is the laser (scattered) field and $\frac{\partial \chi}{\partial \epsilon}$ is the variation of the electric susceptibility with strain (ϵ). The strain generated by the acoustic phonon is defined as $\Delta\epsilon = \frac{\partial u(z)}{\partial z}$, where $u(z)$ is the phonon displacement. The electric susceptibility can be written in a simplified form as[17]

$$\chi(\omega) \propto \frac{|H_{cv}|^2}{\omega_{cv}(\omega_{cv}^2 - \omega^2)}, \tag{2}$$

with the nominator corresponding to the square matrix element of the radiation-matter Hamiltonian between the valence band and the electron states (H_{cv}) and the denominator basically reflecting a resonance at the interband energy $\hbar\omega_{cv}$. The change in electric susceptibility $\frac{\partial \chi}{\partial \epsilon}$ induced by the acoustic phonon thus has three terms, as follows:

$$\frac{\partial \chi}{\partial \omega_{cv}} \frac{\partial \omega_{cv}}{\partial \epsilon}\bigg|_F + \frac{\partial \chi}{\partial \omega_{cv}} \frac{\partial \omega_{cv}}{\partial F} \frac{\partial F}{\partial \epsilon} + \frac{\partial \chi}{\partial |H_{cv}|^2} \frac{\partial |H_{cv}|^2}{\partial F} \frac{\partial F}{\partial \epsilon}, \tag{3}$$

which reflect either the phonon modulation of the transition energy (first two) or of the transition probability (third term).

The first term in Eq. (3) describes the standard deformation potential interaction.[17] Here, we would like to emphasize that the resonant contribution to the susceptibility responsible for the Raman anomalies presented in Figs. 1 and 2 is a function of the built-in fields (F). In fact, it is zero when the fields are absent (e.g., for the [001] samples) or when they are screened by photoexcited carriers (as for the [311] samples at high excitation powers). This field dependence $\chi(F)$ equally applies to both this first photoelastic term and to the other two contributions. In addition, the latter possess explicit field dependencies. In the second term of Eq. (3), $\frac{\partial \omega_{cv}}{\partial F}$ and $\frac{\partial F}{\partial \epsilon}$ are related to the electro-optic and piezoelectric constants, respectively. This term accounts for the piezoelectric mechanism in bulk materials, which is usually weak for III-V compounds. In contrast and as follows from the huge laser-power dependence of the resonant transition observed for the [311] structure in Fig. 4, this term may provide an important contribution in our strained SLs with built-in fields. Similarly, the third term in Eq. (3) is usually disregarded because strain alone *does not* significantly modify the optical transition probabilities. This is, however, clearly not the case when forbidden transitions are considered, as is our case here. In fact, by assuming that the matrix element corresponding to the studied forbidden transition linearly depends on the applied electric field F, $|H_{cv}|^2 = \frac{\gamma}{2} F^2$ (this is the case for the $hh_2 \rightarrow e_1$ transition), it follows that $\frac{\partial |H_{cv}|^2}{\partial \epsilon} = \frac{\partial |H_{cv}|^2}{\partial F} \frac{\partial F}{\partial \epsilon} = \gamma F \frac{\partial F}{\partial \epsilon}$. That is, a term proportional to the built-in field appears, which reflects the change in optical transition probability induced by the acoustic phonon modulation of the electric field. As apparent from Fig. 4, the transition probability is strongly sensitive to the applied field and, thus, such a term can also make a sizable contribution to the Raman cross section. A similar argument can be used to demonstrate that also the second term in Eq. (3) should lead to a contribution proportional to F. We note that the acoustic phonons that should scatter more effectively through the electron-acoustic phonon interactions described above [second and third terms in Eq. (3)] are those with wave vector that matches the periodicity of the permanent built-in fields. These correspond to the first zone-center folded phonons, which is in agreement with the maxima of the broad contributions described in Figs. 1 and 2.

Some simple calculations of $\frac{\partial \omega_{cv}}{\partial \epsilon}\big|_F$ and $\frac{\partial \omega_{cv}}{\partial F} \frac{\partial F}{\partial \epsilon}$ can be performed to estimate the relative weight of the two first terms in Eq. (3). $\frac{\partial \omega_{cv}}{\partial \epsilon}\big|_F$ in the photoelastic contribution is simply the deformation potential, which for GaAs is given by ≈ -8.3 eV (electron plus hole contribution).[19] The piezoelectric constant, on the other hand, gives again for GaAs, $\frac{\partial F}{\partial \epsilon} = 1.4 \times 10^7$ V/cm.[20] This term could be more than an order of magnitude larger for other more polar materials as, e.g., the nitrides.[6,7] Concerning $\frac{\partial \omega_{cv}}{\partial F}$, this term will be strongly dependent on the specific phenomena leading to the electro-optic modulation. From the experimentally observed strong luminescence shift of ≈ 60 meV and assuming that at the highest laser powers used the field is fully screened, we can derive a conservative estimate $\frac{\partial \omega_{cv}}{\partial F} \approx \frac{\Delta \omega_{cv}}{\Delta E} = 1.2 \times 10^{-6}$ eV cm/V. Thus, $\frac{\partial \omega_{cv}}{\partial F} \frac{\partial F}{\partial \epsilon} \approx 17$ eV, which leads to a contribution larger by a factor of 2 [4 in the Raman cross section, Eq. (1)], as compared to the standard photoelastic mechanism. In more general terms, the Stark shift in a QW in the presence of a field F is of the order of $\Delta\omega_{cv} \approx qFL$, where q is the electron charge and L is the well thickness. Thus, $\frac{\partial \omega_{cv}}{\partial F} \approx qL$. For example, for a typical $Ga_{0.85}In_{0.15}As/AlAs$ QW with thickness $L = 100$ Å, this gives $\frac{\partial \omega_{cv}}{\partial F} \approx 10^{-6}$ eV cm/V, which leads again to a contribution to the Raman scattering by acoustic phonons larger than that due to the standard photoelastic mechanism.

In summary, we have observed resonant Raman scattering from acoustic phonons induced by built-in electric fields. The resonant Raman process can be bleached out by screening the built-in fields through the injection of electron-hole pairs. Disorder and probably also inhomogeneities in the built-in electric fields lead to wave vector nonconservation and hence to scattering by phonons from the whole Brillouin zone. A mechanism of acoustic phonon Raman scattering is proposed that derives from the modulation of the optical transition probability and of the transition energy by the

acoustic phonon strain in the presence of built-in electric fields. This mechanism is shown to be proportional to the magnitude of the built-in fields. Although the experiments do not allow us to discriminate between these mechanisms and the deformation potential contribution, basic calculations yield a factor of at least 4 of the former with respect to the latter. The described electron-acoustic phonon interaction could be relevant to other phenomena in piezoelectric strained nanostructures.

We acknowledge Karine Meunier for PLE measurements on the reported samples that helped to identify the involved electronic states. Support from SECyT-ECOS is also acknowledged.

*afains@cab.cnea.gov.ar

†Present address: ATR Laboratories, Sharp Corporation, 2613-1, Ichinomoto, Tenri, Nara 632-8567, Japan.

[1] D. Bria, B. Djafari-Rhouhani, A. Bousfia, E. H. El Boudouti, and A. Nougaoui, Europhys. Lett. **55**, 841 (2001).

[2] N. M. Stanton, R. N. Kini, A. J. Kent, M. Henini, and D. Lehmann, Phys. Rev. B **68**, 113302 (2003).

[3] M. Trigo, A. Bruchhausen, A. Fainstein, B. Jusserand, and V. Thierry-Mieg, Phys. Rev. Lett. **89**, 227402 (2002).

[4] N. D. Lanzillotti Kimura, A. Fainstein, and B. Jusserand, Phys. Rev. B **71**, 041305(R) (2005).

[5] A. J. Kent, R. N. Kini, N. M. Stanton, M. Henini, B. A. Glavin, V. A. Kochelap, and T. L. Linnik, Phys. Rev. Lett. **96**, 215504 (2006).

[6] C.-K. Sun, J.-C. Liang, and X.-Y. Yu, Phys. Rev. Lett. **84**, 179 (2000).

[7] Ümit Özgür, Chang-Won Lee, and Henry O. Everitt, Phys. Rev. Lett. **86**, 5604 (2001).

[8] G. D. Sanders, C. J. Stanton, and C. S. Kim, Phys. Rev. B **64**, 235316 (2001); **66**, 079903(E) (2002); see also G.-W. Chern, K.-H. Lin, C.-K. Sun, J. Appl. Phys. **95**, 1114 (2004).

[9] B. A. Glavin, V. A. Kochelap, T. L. Linnik, and K. W. Kim, Phys. Rev. B **71**, 081305(R) (2005).

[10] G. Rozas, M. F. Pascual Winter, A. Fainstein, B. Jusserand, P. O. Vaccaro, S. Saravanan, and N. Saito, Phys. Rev. B **72**, 035331 (2005).

[11] L. De Caro and L. Tapfer, Phys. Rev. B **51**, 4374 (1995).

[12] Z. V. Popovic, J. Spitzer, T. Ruf, M. Cardona, R. Nötzel, and K. Ploog, Phys. Rev. B **48**, 1659 (1993).

[13] B. Jusserand and M. Cardona, in *Light Scattering in Solids V*, edited by M. Cardona and G. Güntherodt (Springer, Heidelberg, 1989), p. 49.

[14] We have basically observed the same behavior of the resonant spectra in a two laser experiment in which electron-hole pairs are injected, with varying density, by a second laser at higher energies. However, the appearance of a much more intense photoluminescence in this latter case masks out the subtle details displayed in the simpler experiment shown in Fig. 2.

[15] See, for example, T. Ruf, J. Spitzer, V. F. Sapega, V. I. Belitsky, M. Cardona, and K. Ploog, Phys. Rev. B **50**, 1792 (1994), and references therein.

[16] H. Haug and S. W. Koch, *Quantum Theory of the Optical and Electronic Properties of Semiconductors* (World Sientific, London, 1993).

[17] P. Y. Yu and M. Cardona, *Fundamentals of Semiconductors: Physics and Material Properties* (Springer, Berlin, 2003).

[18] I. Sela, D. L. Smith, S. Subbanna, and H. Kroemer, Phys. Rev. B **46**, 1480 (1992).

[19] I. Vurgaftman, J. R. Meyer, and L. R. Ram-Mohan, J. Appl. Phys. **89**, 5815 (2001).

[20] G. Harbeke, O. Madelung, and U. Rössler, *Semiconductors: Physics of Group IV Elements and III-V Compounds*, edited by O. Madelung, Landolt-Börnstein, New Series, Group III, Vol. 17, Pt. A (Springer-Verlag, Berlin, 1982).